Characterization of porosity, structure, and mechanical properties of electrospun SiOC fiber mats

Anran Guo[1,2] · Martina Roso[1] · Michele Modesti[1] · Eric Maire[4] · Jérôme Adrien[4] · Paolo Colombo[1,3]

Abstract In this study, silicon oxycarbide (SiOC) ceramic fiber mats obtained by electrospinning of two different preceramic polymers (MK and H44 resin) were evaluated in terms of their total porosity and other structural characteristics using three different characterization tools. The tensile strength and the permeability of the fiber mats were also investigated. The results indicated that the porosity could be easily calculated based on the apparent density and true density of the fiber mats obtained by gas pycnometry. A modified mercury intrusion porosimetry, in which the bulk volume of the fiber mats was calculated based on its independently measured bulk density, also allowed for an accurate evaluation of the porosity and the pore size distribution of the fiber mats. X-ray computed tomography was able to provide various structural characteristics of the 3D morphology of the fiber mats, but it was less effective in the determination of the total porosity due to resolution limits. All results showed that the MK-derived SiOC fiber mats possessed a higher porosity than the H44-derived SiOC fiber mats, resulting in a higher gas permeability. The ceramic fiber mats possessed a suitable permeability for filtration applications in harsh environments.

✉ Anran Guo
arguo@tju.edu.cn

Martina Roso
martina.roso@gmail.com

Michele Modesti
michele.modesti@unipd.it

Eric Maire
eric.maire@insa-lyon.fr

Jérôme Adrien
jerome.adrien@insa-lyon.fr

Paolo Colombo
paolo.colombo@unipd.it

1 Department of Industrial Engineering, University of Padova, via Marzolo 9, 35131 Padua, Italy

2 School of Materials Science and Engineering, Tianjin University, Tianjin 300072, China

3 Department of Materials Science and Engineering, The Pennsylvania State University, University Park, PA 16801, USA

4 Université de Lyon, INSA-Lyon, MATEIS, CNRS UMR5510, 69621 Villeurbanne, France

Introduction

Fibers are an important class of materials that have been used in various industrial fields; besides the traditional melt-spinning method, many up-and-coming methods including centrifugal jet spinning [1, 2], electrocentrifugal spinning [3], and electrospinning [4, 5], have been used to fabricate micro- or nano-sized fibers. Although the yield of electrospinning is quite limited (few kilograms per hour) due to the delicate spinneret designs with relatively small orifice diameters as well as the need to have low feed rates, electrospinning still is gaining increasing attention due to its easiness in producing almost all kinds of fibers (polymer, ceramic, metallic, and composite fiber) with various shapes, such as hollow fibers and aligned fibers [6, 7]. In a typical electrospinning process, the polymeric fluid is extruded from the orifice of a needle to form a small droplet in the presence of an electric field. When the electric field

is sufficiently strong, charges built up on the surface of the droplet will overcome the surface tension to induce the formation of a liquid jet that is subsequently accelerated toward a grounded collector. As the solvent is evaporating, this liquid jet is stretched to many times its original length to produce continuous fibers of the polymer. Changing the processing parameters, such as solution concentration, applied voltage, and feeding rate, electrospinning is capable of controlling the individual fiber diameter (from tens of nanometers to several micrometers) and the 3D arrangement of the prepared individual fibers (accordingly controlling the porosity characteristics of the fiber mats), ultimately influencing almost all the properties of the fabricated fiber mats [8, 9]. For electrospun fiber mats, the fibers' size and distribution can be determined by evaluating scanning electron microscopy (SEM) micrographs using an image analysis software. However, the characterization tools available for precisely determining the amount of porosity present in electrospun fiber mats are still underdeveloped, and different methods have been reported in the literature. In Xu's work [10], the porosity of poly(L-lactide) electrospun fiber mats was calculated on the basis of their bulk density (based on dimension and weight measurements) and true (theoretical) density. This approach, which we can label as the "bulk density method," has been demonstrated to be quite simple and suitable for almost all kinds of electrospun fiber mats [11]. Besides the bulk density method, mercury intrusion porosimetry (MIP) is another method commonly employed to estimate the porosity of electrospun fiber mats [12, 13]. With the development of technology, researchers tried to use some other novel techniques to calculate the sample's porosity. For example, Manickam and McCutcheon [14] employed the X-ray computed tomography (X-CT) to determine the porosity of polyester nonwovens, and Barolo and colleagues [15] applied the image analysis method to evaluate the porosity of a poly(acrylonitrile-co-vinyl acetate) electrospun fiber mats. Hutten [16] and Manickam and McCutcheon [14], respectively, discussed the existing and emerging methods used for the characterization of the porosity of nonwoven fiber mats. However, the test samples they investigated included both electrospun fiber mats and other kinds of fiber mats; furthermore, they mainly focused on the characterization methods and did not investigate the influence of the porosity on the properties of the fiber mats.

SiOC ceramics constitute a new class of amorphous solid materials derived from the parent structure of silica glass in which the divalent oxygen atoms are partially substituted by tetravalent carbon atoms [17]. Because of the introduction of the carbon atoms, SiOC ceramics possess enhanced thermal, mechanical, and chemical properties compared to pure silica ceramics [18, 19].

Consequently, SiOC glasses with various shapes, such as dense bulk components [20], foams [21], microtubes [22], or fibers [23, 24], have been successfully fabricated to meet the demands of different applications, including high-temperature structural components, protective coatings, and filters.

Our previous paper reported the fabrication of SiOC fiber mats obtained by electrospinning of two different preceramic polymers (MK and H44 silicone resins) [25]. In this work, we focus on the characterization of SiOC fiber mats. Three techniques, including two conventional characterization methods (bulk density method and mercury intrusion porosimetry) and a more innovative technique (X-CT method), were employed to measure the porosity of the two different SiOC fiber mats. The results were compared in order to better understand the limitations and differences among these methods. Furthermore, the relationship between the porosity of the fiber mats with other properties (permeability and mechanical strength) was also investigated.

Experimental

Fabrication process

Two different commercially available silicone resins (MK and H44, Wacker-Chemie GmbH, München, Germany), of similar characteristics but different composition in terms of total carbon content [26], were used as the preceramic precursors, and polyvinylpyrrolidone powder (PVP, $M_w = 1.300.000$ g/mol) was used as the electrospinning assistance because it has high solubility in a variety of solvents and good compatibility with many metal alkoxides. The detailed fabrication process was reported in our previous paper [25]. For the preparation of MK resin electrospinning solution, isopropanol was selected as the electrospinning solvent for the MK resin due to its high solubility for both MK resin and PVP. A certain amount of N,N-dimethylformamide (DMF) was added into the solvent in order to adjust the resultant fiber diameter. In the final fabrication process, 2.7 g of MK resin, 0.9 g of PVP, and 0.06 g of dibutyltin dilaurate (as cross-linking catalyst) were dissolved in a mixture of 8 ml of isopropanol and 2 ml of DMF.

For the fabrication of electrospun H44 fibers, DMF was selected as the electrospinning solvent for H44 resin due to its high solubility for both H44 resin and PVP. A certain amount of chloroform was added to prevent the formation of beads and also adjust the fiber diameter. In the final fabrication process, 3.0 g of H44 resin, 1.0 g of PVP, and 0.5 g of Zr-acetylacetonate (as cross-linking catalyst) were dissolved in a mixture of 5 ml of chloroform and 5 ml of

DMF. All chemicals were purchased from Sigma-Aldrich apart from the dibutyltin dilaurate, purchased from Air Products Chemical. The fibers were fabricated using a typical parallel electrospinning setup, in which the orientation of nozzle was parallel to the horizon. The electrospinning solution was loaded into a 5-ml syringe fitted with a 0.7-mm-diameter stainless steel needle and fed at 0.5 ml/h with a syringe pump (NE-300, New Era Pump Systems, USA). Electrospinning was carried out at a voltage of 10 kV using a DC power supply (ES100R-20 W, Kansai Electronics, Japan). An aluminum plate was used as the collector, and the nozzle–collector distance was 12 cm.

After the spinning process, the as-spun MK/PVP and H44/PVP fibers were cross-linked at 200 °C for 1 h in air to make them infusible. Then the fibers were pyrolyzed in an alumina tube furnace under flowing argon at 1000 °C, with a heating rate of 2 °C/min and a holding time of 2 h. The pyrolyzed samples from the MK and H44 resins were labeled as MK-derived SiOC fiber mats and H44-derived SiOC fiber mats, respectively.

Characterization

Morphology and fiber diameter

The morphology of the fiber mats was examined by a scanning electron microscope (SEM; JSM-6490, Jeol Italia, Italy), after gold coating. The average fiber diameter was determined based on the SEM micrographs using an image analysis software (ImageJ, Research Services Branch, National Institutes of Health, Bethesda, MD, USA). At least 50 diameter measurements were collected per each digitized micrograph.

Porosity

The total porosity of the SiOC fiber mats was measured with three different methods on the same set of samples.

Bulk density method In this method, the total porosity of the electrospun fiber mats was calculated on the basis of their bulk density (ρ) and true density (ρ_0), with the bulk density ρ calculated by dividing the weight by the volume, and ρ_0 measured by gas pycnometry (AccuPyc 1330, Micromeritics Instrument corporation, USA) using helium. During the calculation of sample volume, the thickness of the fiber mats was measured by a micrometer (Mitutoyo Products, Japan) with the resolution of 0.001 mm. Several measurements on different regions of one sample were performed, in order to obtain an accurate average value, and care was taken to not deform significantly the fiber mats while measuring. The porosity values obtained are an average of 10 measurements; the reproducibility is reported

to be within 0.02 % of sample chamber volume, and the accuracy is reported to be within 0.03 % of the volume readings [27].

Mercury intrusion porosimetry (MIP) A mercury intrusion porosimeter (Porosimeter 2000, Carlo Erba Instruments, Italy) was used to analyze the pore structure of the fiber mats. The pore size can be determined based on the external pressure needed to force the liquid into a pore against the opposing force of the surface tension of the liquid, according to the well-known Washburn equation. As the pressure increases during the measurement, the pore size is calculated for each pressure point according to the Washburn equation, and its pore volume is equal to the corresponding volume of the mercury required to fill those pores. Therefore, the pore size distribution can be determined from the volume of the mercury intruded using a range of pressures, and the porosity is determined based on the total volume of the intruded mercury. Each sample was measured three times to ensure reproducibility. The surface tension and contact angle used for mercury were 480 N/m and 141.3°, respectively.

X-ray computed tomography (X-CT) X-CT is a nondestructive technique for obtaining digital information on the sample's 3D architecture and morphological features. It uses the computer-processed X-rays to produce tomographic images or "slices" of specific areas of the body. Then a three-dimensional image is built by stacking a large series of axial slices.

The X-ray computed tomography images of the electrospun SiOC fiber mats were obtained using a high-resolution laboratory tomograph already used and described in our previous work [28]. For this analysis, the voxel size in the reconstructed images was equal to 0.6 μm. It can be asserted that the physical size of the source of the tube is maintained below 0.6 μm because the X-ray tube uses a LaB_6 filament with a very small size, and therefore geometrical blur was not an issue. The acceleration current voltage and intensity were 90 kV and 200 μA, respectively.

Gas permeability

Gas permeability was measured under a nitrogen flow (CFP-1200-A PMI capillary flow porometer, Porous Materials, Inc., USA) on disks with a diameter of 35 mm (see Fig. 1a). The permeability constants were fitted from Forchheimer's equation, expressed as

$$\frac{P_a^2 - P_b^2}{2P_b L} = \frac{\mu}{k} v_s,$$

in which P_a and P_b are, respectively, the absolute gas pressures at the entrance and exit of the sample, v_s is the
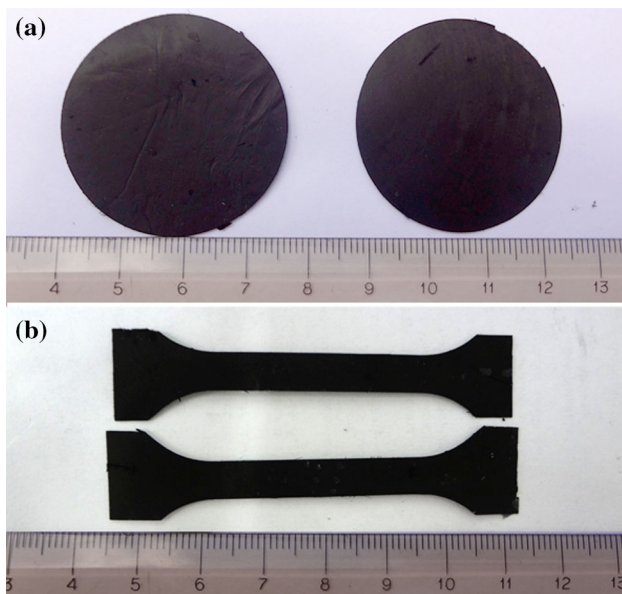
(a)

(b)

Fig. 1 Photographs of the SiOC fiber mats used for the measurement of **a** permeability and **b** tensile strength

superficial fluid velocity, determined by $v_s = Q/A$, where Q is the volumetric flow rate and A is the exposed surface area of the porous medium perpendicular to the flow direction, L is the sample thickness (~ 0.2 mm in the case of the fiber mats characterized in this work), μ is the gas viscosity (1.77×10^{-5} Pa s), and F is the gas density (1.15 kg/m^3) [29].

Tensile strength

The tensile strength of the fiber mats was measured using an ElectroForce planar biaxial test bench test instrument (Bose GmbH, ElectroForce Systems Group, Friedrichsdorf, Germany). The stress was applied uniaxially with a stretching rate of 0.5 mm/min, and the shape of the test fiber mats was prepared according to the ISO 527-3 standard, as shown in Fig. 1b.

Results and discussion

Diameter of the fibers

The formation of the as-spun silicon resin fibers during the electrospinning process and the transformation of the silicon resin into an SiOC ceramic during the pyrolysis process were described in a previous paper [25]. The previous work also demonstrated that the prepared MK-derived and H44-derived SiOC fibers exhibited, after pyrolysis, an uniform morphology with an average fiber diameter of 0.97 ± 0.07 and 1.07 ± 0.08 μm, respectively, and the cross-section of the fibers did not contain any macroscopic defect [25]. Due to the non-uniform geometry of the pores (see Fig. 2), it is impossible to define a single characteristic dimension for them. However, the dimension of the pore size in the SiOC fiber mats appeared to range from ~ 1 to ~ 15 μm, according to SEM images.

Porosity of the fiber mats

The bulk density of a body is defined as the ratio between its mass and the total volume, which includes the volume of the solid part as well as the volume of both open and closed porosity. This is typically obtained from simple geometrical measurements and, from it, the value of the total (or bulk) porosity can be obtained, which is the sum of the open and closed porosity present in the sample. The apparent density of a body is the ratio of the mass of the body to its apparent solid volume, which is constituted by the volume of the solid material plus the volume of the closed pores. Linked to this value is the apparent (or open) porosity, which is the ratio of the volume of the open pores to the bulk volume of the material and is often measured by liquid or gas infiltration techniques. The true (or skeleton) density of a material is equal to the ratio of the mass of the material divided by the volume of the solid material only and corresponds to the density of the same material without any pores. If the value for the apparent density is the same

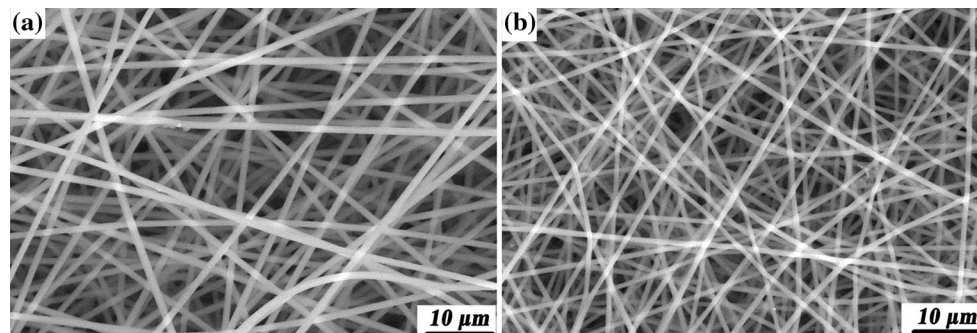**(a)** **(b)**

10 μm   10 μm

Fig. 2 SEM images of the prepared **a** MK-derived and **b** H44-derived SiOC fiber mats

as that for the bulk density, it means that the material does not contain any open pores. If the value for the apparent density is the same as that for the true density, it means that the material does not contain any closed pores. If the value of the bulk density is the same as the value of the true density, the materials does not contain any pores [30].

It should be mentioned that the prepared SiOC fibers in this paper were dense and no closed porosity was present [25]; therefore, the amount of open porosity in the samples corresponded to the amount of total porosity, and the value for the apparent density is the same as that for the true density. In the following sections, three different methods were adopted to characterize the total porosity of the MK-derived and H44-derived SiOC fiber mats.

Bulk density method

The bulk density method is one of the most universal methods to estimate a sample's total porosity based on its weight, volume, and true density. It should be mentioned that, in some works, the authors often use the theoretical density of the material to replace the true density of the fibers [31]. However, most samples are not perfect single crystals, and therefore the true density of the fiber mats is quite different from its theoretical density. In order to eliminate this inaccuracy, we used a pycnometer to measure the fiber's actual true density instead of simply using the theoretical density. The pycnometer results showed that the true densities of MK-derived and H44-derived SiOC fibers were quite similar, despite being produced from different starting materials, and were 2.0985 ± 0.0008 and 2.1079 ± 0.0013 cm^3/g, respectively. These values are in line with published values for dense polymer-derived ceramics (2.1 cm^3/g) [17], although this characteristic strongly depends on the thermal history of the material (processing temperature, dwelling time, and heating rate).

The bulk densities of the MK-derived and H44-derived SiOC fiber mats were calculated by measuring their weight and the corresponding volumes, which were 0.163 ± 0.009 and 0.191 ± 0.005 cm^3/g, respectively. The total porosities of the MK-derived and H44-derived SiOC fiber mats, calculated using the bulk density method, were 92.21 ± 0.48 and 90.91 ± 0.26 vol%, respectively. This difference in porosity value can be attributed to the different electrospinning parameters, especially the electrospinning solvent as described in the "Experimental" section, adopted in the electrospinning process that influenced the 3D arrangement of the SiOC fibers in the nonwoven fiber mats.

Mercury intrusion porosimetry (MIP)

Mercury intrusion porosimetry is another quite common method to characterize the (open) porosity of a body.

Figure 3 reports the typical mercury injection curve for the MK-derived and H44-derived SiOC fiber mats. Comparing the two curves, it can be seen that when all pores in two kinds of fiber mats were filled with mercury, the volume of the infiltrated mercury per unit mass of the MK-derived SiOC fiber mats was higher than the one infiltrated in per unit mass of the H44-derived SiOC fiber mats. This indicates that the total pore volume in per unit mass of the MK-derived SiOC fiber mats was higher than that present in per unit mass of the H44-derived SiOC fiber mats. Because the bulk densities of two fiber mats were quite similar, around 2.1 cm^3/g, it can be concluded that the porosity of the MK-derived SiOC fiber mats was higher than that of the H44-derived SiOC fiber mats. On the basis of the mercury injection curve, the porosities of the MK-derived and H44-derived SiOC fiber mats resulted to be 74.75 ± 1.12 and 73.14 ± 0.94 vol%, respectively. However, these values were much smaller than those obtained using the bulk density method. We attribute this difference to the inaccuracy in the determination of the samples' apparent volume, as calculated by MIP. The porosity calculation process by MIP, in fact, is based on the formula: Porosity $= V_{pore}/(V_{pore} + V_{apparent})$, where "Porosity" is the value for the apparent porosity, V_{pore} is the total pore volume of the test sample, and $V_{apparent}$ is the apparent volume of the test sample. For the MIP technique, the pore size is determined based on the external pressure needed to force the liquid into a pore according to the Washburn equation, and its corresponding pore volume is equal to the volume of mercury required to fill these pores. Therefore, the total pore volume of the sample (V_{pore}) is equal to the total volume of the infiltrated mercury, and this can be easily obtained from the typical mercury injection curve (Fig. 3). However, the measurement of the apparent volume ($V_{apparent}$) is more complicated; normally, the $V_{apparent}$
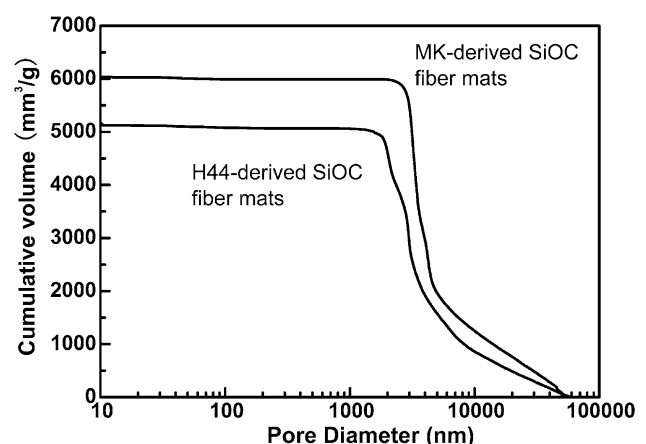

Fig. 3 Typical mercury injection curves for the MK-derived and H44-derived SiOC fiber mats

is calculated according to the difference between the weight of mercury used when the test chamber is fully filled by the mercury with and without adding the test sample. Therefore, in order to obtain an accurate value for the calculated apparent volume, the tested sample should possess a certain volume and mass, normally requiring the weight of tested sample to be higher than 500 mg. However, due to the nonwoven loose structure of the electrospun fiber mats, the weight of the tested SiOC fiber mats could only reach 60 mg when the test chamber was completely filled with it, leading to inaccuracies in the determination of the apparent volume as calculated by the MIP technique. Based on the above considerations, we can consider that the total pore volume of the sample measured by MIP is correct, while the apparent volume of the sample given by MIP is erroneous. Therefore, we suggest that, in the case of our samples, the apparent volume could be calculated based on their apparent density and weight, as described in the following equation, instead of directly adopting the value obtained using the MIP technique:

$$
\text{Porosity \%} = \frac{V_{pore}(\text{cm}^3)}{V_{pore}(\text{cm}^3) + V_{apparent}(\text{cm}^3)} \times 100 \%
$$
$$
= \frac{V_{infiltrated}(\text{cm}^3/\text{g})}{V_{infiltrated}(\text{cm}^3/\text{g}) + [\rho_{apparent}(\text{g/cm}^3)]^{-1}} \times 100 \%,
$$

where $V_{infiltrated}$ is the volume of the infiltrated mercury in per unit mass sample and $\rho_{apparent}$ is the apparent density of the sample. In this work, the data of $V_{infiltrated-MK}$ and $V_{infiltrated-H44}$ were the Y-axis value of the crossing point between the Y-axis and the mercury injection curve in Fig. 3, being 6057.94 and 5211.71 mm³/g, respectively, and the apparent density values of the samples are equal to the true density values measured by pycnometry as described in "Bulk density method" section. Inserting these data in the equation, we obtain apparent porosities of the MK-derived and H44-derived SiOC fiber mats of 92.71 ± 0.04 and 91.65 ± 0.05 vol%, respectively. This result is quite similar to that found using the bulk density method. Therefore, we can state that the modified MIP method can provide an accurate porosity value for electrospun fiber mats.

Besides the porosity value, the typical mercury injection curve (Fig. 3) was also able to provide the information about the pore size distribution because the volume of the mercury intruded under a certain pressure was equal to the corresponding pore volume. Figure 4 shows the pore size distribution of MK-derived and H44-derived SiOC fiber mats. It reveals that two SiOC fiber mats exhibit similar pore size distribution, mainly ranging from 1 to 6 µm, and the average pore size of MK-derived SiOC fiber mats was slightly larger than that of H44-derived SiOC fiber mats.
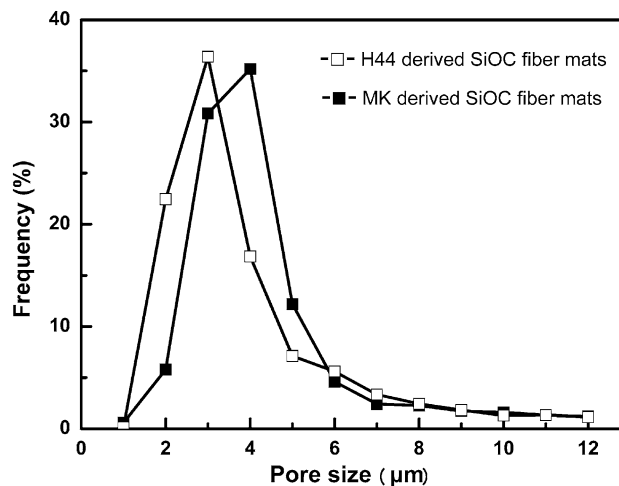

Fig. 4 Pore size distribution of the MK-derived and H44-derived SiOC fiber mats obtained by MIP

X-ray computed tomography (X-CT) method

X-CT can provide a 3D structure of the tested sample by reconstructing the 2D images of each of the sample's layers (each slice). Figure 5 shows the images of the 3D structure of the MK-derived and H44-derived SiOC fiber mats obtained by ray tracing after a simple threshold of the initial 3D gray-level images, revealing a typical nonwoven structure (see video 1 and video 2 in the "Supplementary Material Section" for the detailed information). The gray level in the fibers is much higher than that in the porosity, so the
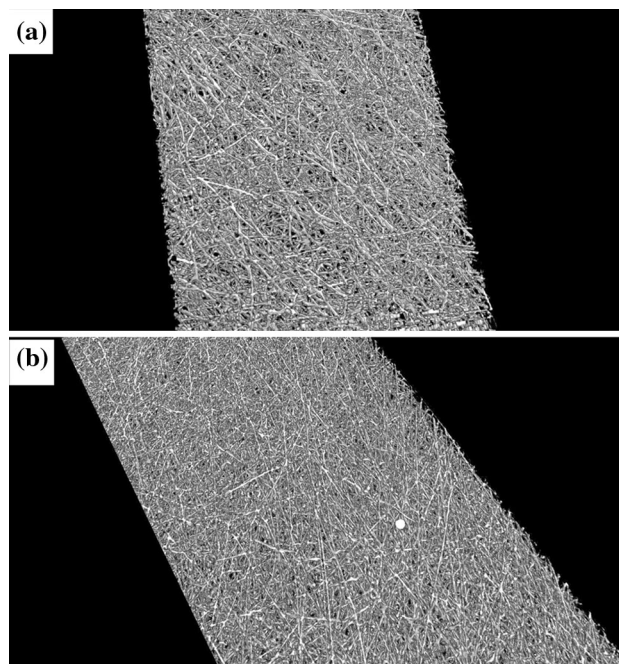

Fig. 5 Reconstruction, from X-CT data, of the 3D structure of the **a** MK-derived and **b** H44-derived SiOC fiber mats

thresholding process is rather straightforward. The subsequent image processing, performed using proprietary plugins implemented in the ImageJ software, provided the information about the solid fraction distributions of each slice in the SiOC fiber mats, as shown in Fig. 6. The data indicate that the solid fractions of each slice were almost the same, fluctuating around 13 vol% for MK-derived SiOC fiber mats and around 17 vol% for H44-derived SiOC fiber mats, suggesting that the morphology of the SiOC fiber mats in each slice was quite uniform. This testifies that the fabrication process was stable and well controlled [25]. In Fig. 6, the Y-axis value is the solid fraction of each slice; therefore, the average of every Y-axis data corresponds to the solid fraction of the whole sample, and the resultant porosity of the sample can be calculated by the following equation:

$$Porosity\,\% = 100\,\% - Solid\ fraction\,\%$$
$$= \left(1 - \frac{\sum\limits_{i=0}^{n} y_i}{n}\right) \times 100\,\% ,$$

where y_i is the Y-axis value for each slice and n is the total number of slices (the value of n is 587 in this paper). We can thus obtain that the porosities of MK-derived and H44-derived SiOC fiber mats were 87.67 and 82.48 vol%, respectively. Figure 7 shows the solid fraction distributions of each subvolume ($12 \times 12 \times 12$ μm) in SiOC fiber mats. The total porosity of the two SiOC fiber mats can be calculated by the following equation:

$$Porosity\,\% = 100\,\% - Solid\ fraction\,\%$$
$$= \left(1 - \frac{\sum\limits_{i=0}^{100} x_i y_i}{\sum\limits_{i=0}^{100} y_i}\right) \times 100\,\% ,$$
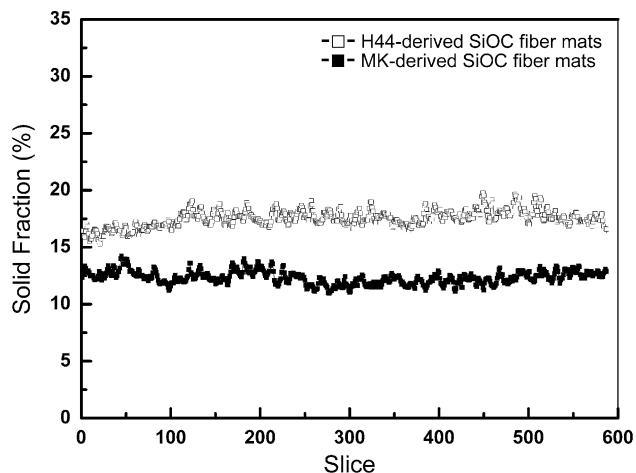

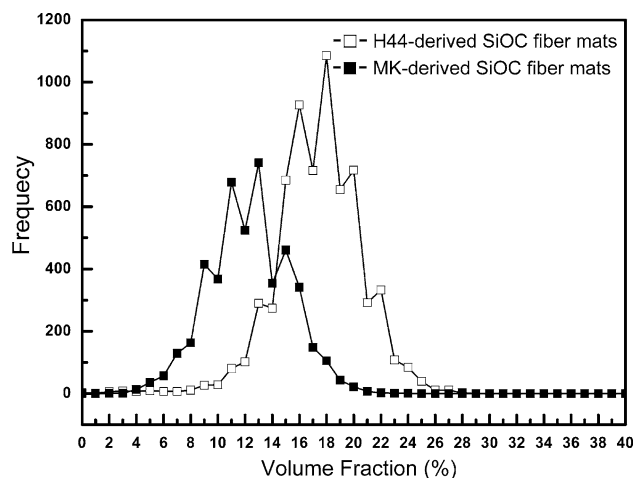**Fig. 6** Solid fraction distributions of each slice in the SiOC fiber mats

Fig. 7 Solid fraction distributions of each subvolume ($12 \times 12 \times 12$ μm) in the SiOC fiber mats

where x_i and y_i are the X-axis value and Y-axis value for each subvolume, respectively. The corresponding porosities of the MK-derived and H44-derived SiOC fiber mats were 87.68 and 82.58 vol%, respectively. This result is almost the same as that calculated according to Fig. 6. This was anticipated because measuring the solid fraction as an average of many slices or of many 3D subvolumes is equivalent if the number of slices and subvolumes is high. It should however be mentioned that these measurements cannot be regarded as absolute. The accuracy of the calculation result is mainly determined by the resolution of the X-CT equipment. Using a well-optimized bench equipment, the maximum resolution was about 0.6 μm; this is a very good achievement for a lab CT, but it is not sufficient to describe the small fibers in the studied materials with a sufficient number of pixels. During the analysis process, the part of the samples recognized as 'solid' by the tomography technique actually contains very fine pores constructed by the fibers; therefore, the number of pores detected by the X-CT were fewer than that detected by MIP, and it is not a surprise to observe that the porosity value measured by X-CT was little lower than the one calculated by the two previous methods.

Besides the solid fraction present in the fiber mats, the X-CT analysis was also able to provide other structural characteristics of the samples. Figure 8 shows the pore size distribution of MK-derived and H44-derived SiOC fiber mats measured by a procedure described in our previous work [32], which is called 3D granulometry, performed by sequential opening operations. Two SiOC fiber mats exhibited a rather similar pore size distribution, ranging from 2 to 12 μm, and the average pore size of MK-derived SiOC fiber mats was larger than that of H44-derived SiOC fiber mats, which is consistent with the result obtained by the MIP method (Fig. 4).
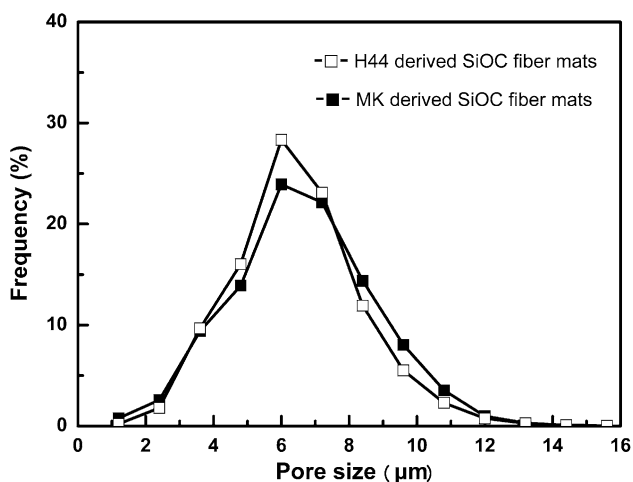
Fig. 8 Pore size distribution of the MK-derived and H44-derived SiOC fiber mats, analyzed by X-CT

A typical structural characteristic of nonwoven fiber mats is that the fibers are randomly oriented in the length and width directions and are deposited layer wise along the thickness. Figure 9 represents the directionality (angle distribution) of each fiber measured in the plane of the mat. The detected histograms should be flat if the fibers in the same plane represent a random orientation. However, the result illustrates that both kinds of fibers had a preferred orientation (this orientation is not quite pronounced because the maximum Y-axis value, frequency, was only 2.5 %). We can attribute this slight preferred orientation to the role of the gravity force during the electrospinning process. The SiOC fibers were fabricated using a typical parallel electrospinning setup, in which the orientation of nozzle was parallel to the horizon. Therefore, during the electrospinning process, the liquid jet was subjected to two forces: the electric force parallel with the horizon and the gravity force perpendicular to the ground. When the liquid
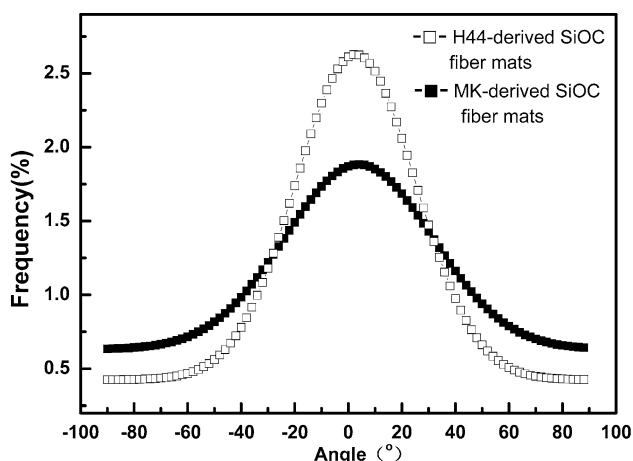

Fig. 9 Directionality (angle distribution) of each fibers for the MK-derived and H44-derived SiOC fiber mats

jet flies toward the collector, the electric force drives the liquid jet to form fibers with a random orientation, while the gravitational force tends to orient the liquid perpendicular to the ground. Therefore, the prepared SiOC fibers show a preferred orientation.

Besides the mentioned three methods, image analysis of SEM micrographs is another potential method to calculate the porosity of a material and has been successfully applied to porous ceramics [33]. Our group has also tried to adopt this method to calculate the porosity of the produced fiber mats; however, during the operation process, we found that it was very difficult to set an appropriate threshold for the electrospun fiber mats, due to their complex architecture. In previous work that used image analysis to calculate the sample's porosity, the microstructure of the test sample was very simple and regular; therefore, it was quite easy to distinguish which part of the image constituted the pores and then set a suitable threshold to transform the SEM image into a binary image [33]. However, for the electrospun fibers, the orientation of the fibers was quite random (see Fig. 2), and therefore it was difficult to threshold the images to clearly delineate where a fiber is or is not present. Because the fibers were somewhat flexible, the method of infiltrating a contrasting agent, such as epoxide resin, into the fiber mats to improve the contrast between fibers and pores was also not suitable for the SiOC fibrous fiber mats. One possible solution would be to use a more professional image analysis software to make a complicated calculation to threshold the electrospun fiber mats SEM image, as described in Tomba's work [15]; however, this is beyond the scope of this study.

Based on the above analysis, we can conclude that the bulk density method was the easiest to conduct and no specialized equipment was required; therefore, this method was also the quickest and the cheapest one for the measurement of the porosity of electrospun fiber mat. However, in order to obtain a more accurate result, it is better to measure the fiber mats' true density by pycnometer instead of directly using the theoretical density, and care should be taken to measure the thickness of the fiber mat. A modified MIP method, in which the bulk volume was calculated based on the bulk density of the fiber mats, could provide a reliable value for the porosity and pore size distribution, and the cost was not too high. High-resolution X-CT was able to visualize the 3D structures of the SiOC fiber mats and with the subsequent image analysis provided many of their structural characteristics, including porosity, pore size distribution, and directionality (angle distribution) of each fiber. However, this method was quite time consuming, requiring several days for one sample, and also expensive. In addition, due to limited resolution, this method was not suitable for the determination of the exact fiber size and size distribution in the nanofiber mat. SEM image analysis

is an attractive method, but more research is required for its optimization.

Tensile strength and permeability

The tensile stress–strain curves for the SiOC fiber mats are shown in Fig. 10, suggesting that the tensile strength of H44-derived SiOC fiber mats and MK-derived SiOC fiber mats were 0.17 ± 0.05 MPa and (0.11 ± 0.03 Mpa), respectively. Figure 11a, b reports the SEM images of the fracture region of MK-derived SiOC fiber mats, revealing that the fiber mats exhibited a laminar fracture, which could also be proved by the ladder-like stress–strain curves for the fiber mats. The fiber mats appear to be constituted by planar layers which are bonded to each other more weakly than the fibers within the same layer because of partial melting of the fibers localized at the contact points (Fig. 11c), occurring during cross-linking when the silicone resin fibers are heated above the glass transition temperature of the polymer (∼42 °C for both resins) [26].

The pressure drop curves for MK-derived and H44-derived SiOC fiber mats are shown in Fig. 12. The corresponding permeability constant k values for MK-derived and H44-derived SiOC fiber mats were
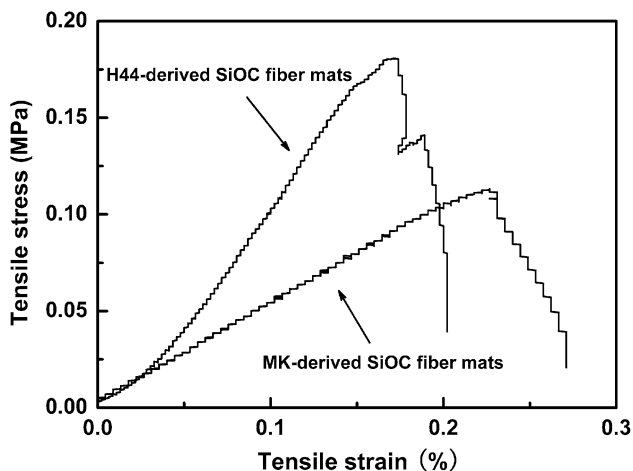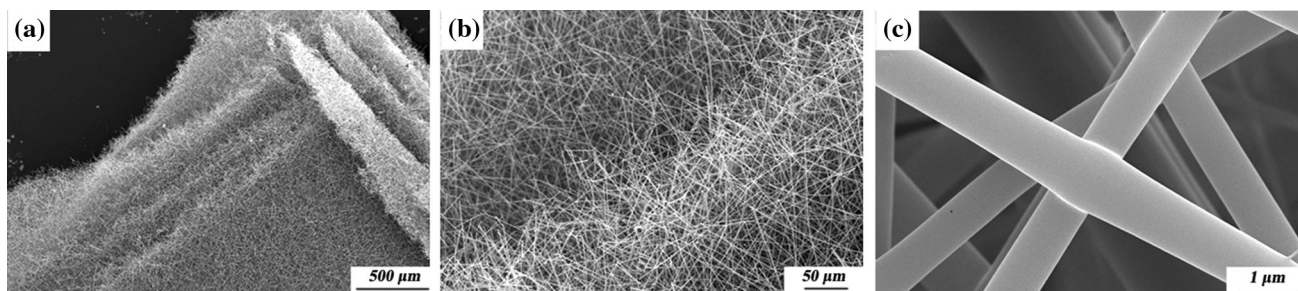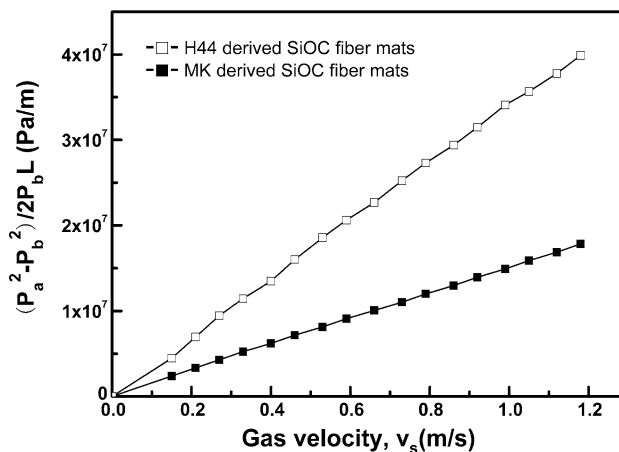

Fig. 12 Pressure drop curves for the SiOC fiber mats

$1.15 \pm 0.09 \times 10^{-12}$ and $5.32 \pm 0.12 \times 10^{-13}$ m^2, respectively, and the higher permeability of the MK-derived SiOC fiber mats is in accordance with its higher porosity. In addition, according to Innocentini et al. [29, 33], the permeability constant of the SiOC fiber mats lies in the region typical for high-efficiency particulate air (HEPA) filters (from 1×10^{-11} to 1×10^{-13} m^2). This indicates that the prepared SiOC fiber mats have a potential application in the filtration field, especially in high-temperature and corrosive environments, since SiOC ceramics have a high thermo-chemical stability [34]. The main characteristics of the investigated fiber mats are reported in Table 1.

Conclusions

In this paper, two different SiOC fiber mats (MK-derived and H44-derived SiOC fiber mats) were produced by electrospinning of preceramic polymers and high-temperature pyrolysis, and their structural characteristics were evaluated by three different methods: bulk density method, MIP method, and X-CT method. Furthermore, the tensile strength and permeability of the fiber mats were also investigated. The bulk density method was the easiest, quickest, and cheapest tool for the determination of the

Fig. 10 Tensile strength of the SiOC fiber mats

Fig. 11 SEM images of the fracture region of the MK-derived SiOC fiber mats

Table 1 Main characteristics of the investigated fiber mats

Characteristic	MK-derived fiber mat	H44-derived fiber mat
Fiber diameter (μm)	0.97 ± 0.07	1.07 ± 0.08
Total porosity (vol%) (bulk density method)	92.21 ± 0.48	90.91 ± 0.26
Total porosity (vol%) (modified MIP method)	92.71 ± 0.04	91.65 ± 0.05
Total porosity (vol%) (X-CT method)	87.68	82.58
Permeability constant (m^2)	$1.15 \pm 0.09 \times 10^{-12}$	$5.32 \pm 0.12 \times 10^{-13}$
Tensile strength (MPa)	0.11 ± 0.03	0.17 ± 0.05

fiber mats' porosity, and no specialized equipment was required; however, in order to get a more accurate result, it is better to measure the fiber mats' true density by pycnometer instead of directly using the theoretical density, and care should be taken to measure the thickness of the fiber mat; MIP could provide a reliable pore size distribution for the fiber mats, but an incorrect porosity value due to the inaccuracy in the determination of the fiber mats' bulk volume, as calculated by MIP. A modified MIP method, in which the bulk volume was calculated based on the bulk density of the fiber mats, allowed to obtain a more accurate value for the porosity. High-resolution X-CT was able to visualize the 3D structures of the SiOC fiber mats and with the subsequent image analysis provided many of their structural characteristics, including porosity, pore size distribution, and directionality (angle distribution) of each fiber. However, this method was quite time consuming and was also very expensive. In addition, due to fact that the resolution of the equipment was similar to the fiber size, the determination of the total porosity was not as accurate as the other analysis methods employed.

All results show that the porosities of two fiber mats were higher than 80 %, and the MK-derived SiOC fiber mats exhibited a higher porosity than the H44-derived SiOC fiber mats. In addition, the permeability constant k values for MK-derived and H44-derived SiOC fiber mats were $1.15 \pm 0.09 \times 10^{-12}$ and $5.32 \pm 0.12 \times 10^{-13}$ m^2, respectively, indicating that the SiOC fiber mats prepared in this work appear to be suitable for filtration applications in harsh environments.

References

1. Mahalingam S, Edirisinghe M (2013) Forming of polymer nanofibers by a pressurised gyration process. Macromol Rapid Commun 34:1134–1139
2. Ren L, Pandit V, Elkin J, Denman T, Cooper JA, Kotha SP (2013) Large-scale and highly efficient synthesis of micro- and nano-fibers with controlled fiber morphology by centrifugal jet spinning for tissue regeneration. Nanoscale 5:2337–2345
3. Khamforoush M, Asgari T (2014) A modified electro-centrifugal spinning method to enhance the production rate of highly aligned nanofiber. NANO. doi:10.1142/S1793292015500162
4. Kaur S, Sundarrajan S, Rana D, Sridhar R, Gopal R, Matsuura T, Ramakrishna S (2014) Review: the characterization of electro-spun nanofibrous liquid filtration fiber mats. J Mater Sci 49:6143–6159. doi:10.1007/s10853-014-8308-y
5. Goh YF, Shakir I, Hussain R (2013) Electrospun fibers for tissue engineering, drug delivery, and wound dressing. J Mater Sci 48:3027–3054. doi:10.1007/s10853-013-7145-8
6. Sigmund W, Yuh J, Park H, Maneeratana V, Pyrgiotakis G, Daga A, Taylor J, Nino JC (2006) Processing and structure relationships in electrospinning of ceramic fiber systems. J Am Ceram Soc 89:395–407
7. Luo CJ, Stoyanov SD, Stride E, Pelan E, Edirisinghe M (2012) Electrospinning versus fibre production methods: from specifics to technological convergence. Chem Soc Rev 41:4708–4735
8. Zhang L, Aboagye A, Kelkar A, Lai C, Fong H (2013) A review: carbon nanofibers from electrospun polyacrylonitrile and their applications. J Mater Sci 49:463–480. doi:10.1007/s10853-013-7705-y
9. Wu H, Pan W, Lin D, Li H (2012) Electrospinning of ceramic nanofibers: fabrication, assembly and applications. J Adv Ceram 1:2–23
10. Xu X, Chen X, Liu A, Hong Z, Jing X (2007) Electrospun poly(L-lactide)-grafted hydroxyapatite/poly(L-lactide) nanocomposite fibers. Eur Polym J 43:3187–3196
11. Luoh R, Hahn HT (2006) Electrospun nanocomposite fiber mats as gas sensors. Compos Sci Technol 66:2436–2441
12. Lowery JL, Datta N, Rutledge GC (2010) Effect of fiber diameter, pore size and seeding method on growth of human dermal fibroblasts in electrospun poly(epsilon-caprolactone) fibrous mats. Biomaterials 31:491–504
13. Bhattarai SR, Bhattarai N, Yi HK, Hwang PH, Cha DI, Kim HY (2004) Novel biodegradable electrospun fiber mats: scaffold for tissue engineering. Biomaterials 25:2595–2602
14. Manickam SS, McCutcheon JR (2012) Characterization of polymeric nonwovens using porosimetry, porometry and X-ray computed tomography. J Membr Sci 407–408:108–115
15. Tomba E, Facco P, Roso M, Modesti M, Bezzo F, Barolo M (2010) Artificial vision system for the automatic measurement of interfiber pore characteristics and fiber diameter distribution in nanofiber assemblies. Ind Eng Chem Res 49:2957–2968
16. Hutten IM (2007) Handbook of non-woven filter media, 1st edn. Butterworth-Heinemann, Oxford
17. Colombo P, Mera G, Riedel R, Sorarù GD (2010) Polymer-derived ceramics: 40 years of research and innovation in advanced ceramics. J Am Ceram Soc 93:1805–1837
18. Sorarù GD, Suttor D (1999) High temperature stability of sol-gel-derived SiOC glasses. J Sol-gel Sci Technol 14:69–74
19. Brewer CM, Bujalski DR, Parent VE, Su K, Zank GA (1999) Insights into the oxidation chemistry of SiOC ceramics derived from silsesquioxanes. J Sol-gel Sci Technol 14:49–68

20. Harshe R, Balan C, Riedel R (2004) Amorphous Si(Al)OC ceramic from polysiloxanes: bulk ceramic processing, crystallization behavior and applications. J Eur Ceram Soc 24:3471–3482

21. Vakifahmetoglu C, Colombo P (2008) A direct method for the fabrication of macro-porous SiOC ceramics from preceramic polymers. Adv Eng Mater 10:256–259

22. Colombo P, Perini K, Bernardo E, Capelletti T, Maccagnan G (2003) Ceramic microtubes from preceramic polymers. J Am Ceram Soc 86:1025–1027

23. Kita K, Narisawa M, Nakahira A, Mabuchi H, Itoh M, Sugimoto M, Yoshikawa M (2009) High-temperature pyrolysis of ceramic fibers derived from polycarbosilane-polymethylhydrosiloxane polymer blends with porous structures. J Mater Sci 45:139–145. doi:10.1007/s10853-009-3905-x

24. Guo A, Roso M, Modesti M, Liu J, Colombo P (2014) Hierarchically structured polymer-derived ceramic fibers by electrospinning and catalyst-assisted pyrolysis. J Eur Ceram Soc 34:549–554

25. Guo A, Roso M, Modesti M, Liu J, Colombo P (2014) Preceramic polymer-derived SiOC fibers by electrospinning. J Appl Polym Sci 131:39836

26. Takahashi T, Kaschta J, Münstedt H (2001) Melt rheology and structure of silicone resins. Rheol Acta 40:490–498

27. Dinger DR (2005) Characterization techniques for ceramists. Morris Publishing, Clemson

28. Etiemble A, Adrien J, Maire E, Idrissi H, Reyter D, Roué L (2014) 3D Morphological analysis of copper foams as current collectors for Li-ion batteries by means of X-ray tomography. Mater Sci Eng, B 187:1–83

29. Biasetto L, Colombo P, Innocentini MD, Mullens S (2007) Gas permeability of microcellular ceramic foams. Ind Eng Chem Res 46:3366–3372

30. Chesters JH (1983) Refractories. Production and properties. The Metals Society, London

31. Zhu X, Cui W, Li X, Jin Y (2008) Electrospun fibrous mats with high porosity as potential scaffolds for skin tissue engineering. Biomacromolecules 9:1795–1801

32. Maire E, Colombo P, Adrien J, Babout L, Biasetto L (2007) Characterization of the morphology of cellular ceramics by 3D image processing of X-ray tomography data. J Eur Ceram Soc 27:1973–1981

33. Innocentini M, Faleiros R, Pisani R Jr, Thijs I, Luyten J, Mullens S (2010) Permeability of porous gelcast scaffolds for bone tissue engineering. J Porous Mater 17:615–627

34. Sorarù GD, Modena S, Guadagnino E, Colombo P, Egan J, Pantano C (2002) Chemical durability of silicon oxycarbide glasses. J Am Ceram Soc 85:1529–1536